IEEE Access
Multidisciplinary | Rapid Review | Open Access Journal

Received 12 July 2023, accepted 10 August 2023, date of publication 17 August 2023, date of current version 24 August 2023.

Digital Object Identifier 10.1109/ACCESS.2023.3305923

APPLIED RESEARCH

Innovative Plug-and-Play System for Electrification of Wheel-Chairs

FEDERICO PACINI[1], STEFANO DI MATTEO[1], PIERPAOLO DINI[1], LUCA FANUCCI[1], (Fellow, IEEE), AND FRANCESCO BUCCHI[2]

[1]Department of Information Engineering, University of Pisa, 56126 Pisa, Italy
[2]Department of Civil and Industrial Engineering, University of Pisa, 56126 Pisa, Italy

Corresponding author: Federico Pacini (federico.pacini@phd.unipi.it)

ABSTRACT Self-propelled wheelchairs are challenging to drive on off-road routes or require enormous physical effort in situations where the gradient exceeds 8%. For most people, these situations are too strenuous and therefore impractical. This work presents an innovative plug-and-play system to electrify a manual wheelchair. With the constraint of not irreversibly modifying the original wheelchair, a mechanical system is developed to allow motors to turn the rear wheels by friction. Torque and power requirements have been derived by modeling and simulating in Matlab the physical system. To manufacture a working prototype, a control system using standard components is devised, and object-oriented firmware is developed with the C++ programming language. The result is a plug-and-play portable kit that can be adapted to wheelchairs of any size, and the expandable Human-Machine-Interface (HMI) makes it ready to expand the audience that can use it.

INDEX TERMS Assistive technology, electrification, wheelchairs, electric mobility, human–machine interface, human empowerment, independent living.

I. INTRODUCTION

A. OVERVIEW & MOTIVATIONS

Eurostat, the statistical office of the European Union, estimates that there are currently 5 million wheelchair users in Europe and this value is likely to increase due to the aging of the population [1]. Among this population, our target group consists of wheelchair users who are able to self-propel their wheelchairs using push-rims mounted on the rear wheels and want to travel. Self-propelled wheelchairs are difficult to drive on off-road routes [2] or require enormous physical effort in situations where the gradient exceeds 8% [3], [4]. For most people, these situations are too strenuous and therefore impractical [5]. There are several options available for wheelchair electrification and propulsion support devices. Each of these options has its pros and cons which can vary according to the specific needs of the user. In general, electrification of wheelchairs can provide greater independence [6], mobility, and well-being [7], without the need for considerable physical effort. Electric-powered wheelchairs (EPWs) can cover long distances and overcome inclines more easily. However, they can be expensive, much heavier, and bulkier than manual wheelchairs, which makes them impractical in some situations [8], e.g. when weight is an issue, such as when using weight-restricted indoor lifts. Furthermore, when travelling by plane, space and battery problems may arise. Moreover, if for any reason the EPW is unable to move independently, the weight of the chair may make manual pushing difficult. Considering our target group, their needs hardly fit the advantages an EPW offers. For the abovementioned reasons, there have been several attempts to manufacture kits to transform a manual wheelchair into EPW. Some of them are available on the market such as [9], [10], [11], [12], [13], and [14]. However, solutions like [9] and [10] add a motorized wheel in front of the wheelchair whereas the center of gravity is shifted backwards toward the rear wheels. In conditions such as unpaved roads, this configuration results in the slipping of the front motorized wheel. Solutions like [11] and [12] require mounting their own compatible wheels. Solutions

The associate editor coordinating the review of this manuscript and approving it for publication was Paolo Giangrande.

such as [13] are likely to be plug-and-play if a support frame is previously mounted on the wheelchair: this may require irreversible modifications to the wheelchair. In addition, the supplied configurations are not powerful enough to cope with steep slopes whose gradient exceeds 8%. Solutions such as [14] require the user to manually control the direction of the wheelchair at all times, and in the case of uneven terrain, it is likely that the motorised rear wheel will not touch the ground properly, causing a discontinuous grip. In literature, there are some attempts to design portable kits like in [15] and [16] but they lack physical implementation and testing.

In this paper, we describe our solution for wheelchair electrification, which combines the advantage of ease of assembly, adaptability on the fly for a wide variety of wheelchairs, capability to tune the mechanical stiffness of the motor supports, and the motorization of rear wheels to take advantage of the adherence of the main wheels, which bear the majority of the weight of the individual being transported. Considering that the kit's primary objective is to enable people with manual wheelchairs to overcome situations where their manual propulsion is insufficient to cope with the environment, the actual speed of the wheelchair and the vertical vibrations to which the user is subjected are comparable to those of a manual wheelchair. For this reason, and because we did not want to modify the structure of the wheelchair, we did not consider any passive or active suspension [17], [18] to reduce the vertical vibrations. Nowadays, to enhance system safety and user experience, attempts to include features from autonomous control such as path-tracking [19] for off-road lane maintenance and motion-planning depending on obstacles [20] are frequent. Anyway, these techniques require the usage of sensors to be aware of the surroundings and would decrease the degree of plug-and-playness. For this reason, we implement only a manual control system.

Discussion and details on mechanical design are presented in Section II. System dynamics, prototype architecture, software architecture, and prototype implementation are summarized in Section III. Finally, Section IV discusses the result and potential applications of our plug-and-play system.

B. MAIN CONTRIBUTIONS

This paper introduces innovative features related to the electrification of manual wheelchairs that overcome some state-of-the-art solutions. The motor frame is lightweight and it can be attached to different wheelchairs since its joints can be adjusted both in height and width to fit a wide variety of wheelchair chassis. In addition, the power transmission is obtained thanks to friction between out-runner motors and wheelchair tires, without requiring any permanent modification of the wheelchair chassis. Concerning electronics and informatics, a control system using off-the-shelf components was devised and software firmware written in C++ was developed and made available on GitHub.

The mechanical design of the device is novel and the authors applied for a patent [21].

II. INNOVATIVE ADAPTIVE SYSTEM DESIGN

From a mechanical point of view, the electrification device has to achieve the following goals: (i) to be interfaced with the wheelchair in a smart and easy way, without requiring any permanent modification of the wheelchair (e.g. no holes have to be carried out on the wheelchair frame); (ii) to be compatible with different wheelchair models and sizes; (iii) to be lightweight.

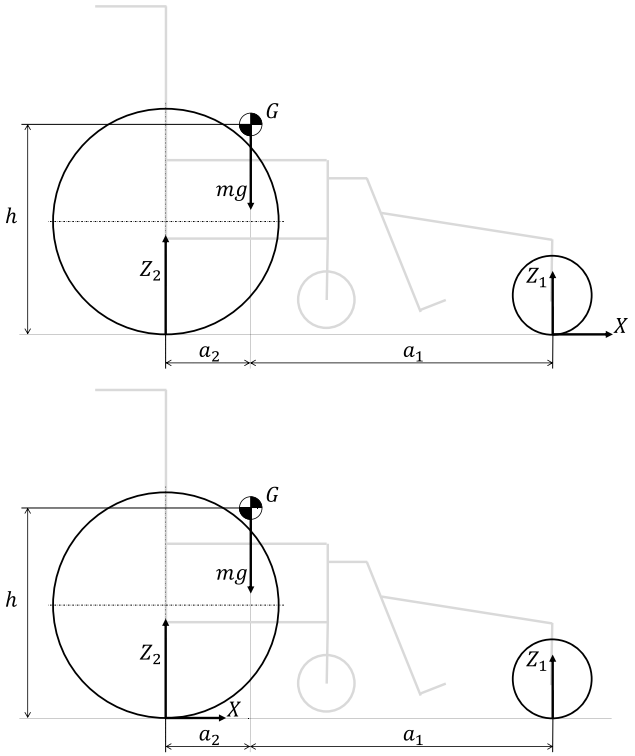

FIGURE 1. Wheelchair equilibrium with the additional front wheel - Powered front wheel (Up) and Powered rear wheels (Down).

A. FRONT-DRIVE VS REAR-DRIVE

In order to compute the performance of the motorized wheelchair, two preliminary designs were considered: (i) a powered additional front wheel and (ii) powered wheelchair rear wheels. Both designs consider an additional front wheel, having a larger diameter than the original wheelchair front wheels, in order to enhance the stability performance on irregular ground. The mechanical equilibrium of both configurations is shown in Fig. 1. The wheelchair and transported person's center of gravity, considered as a unique rigid body, is G. The vertical height of the point G is h while the distance along the horizontal axis between the center of gravity and the front and rear wheels is a_1 and a_2 respectively. The weight due to the total mass (wheelchair and person) m and the gravity acceleration g is considered to be applied in G, and the front and rear vertical forces, Z_1 and Z_2 respectively, are applied at the contact point between the wheel and the ground. The longitudinal force X is applied at the front contact patch, if the powered front wheel layout is

considered or at the rear contact patch, if the powered rear wheels layout is considered.

Two different phenomena limit the maximum longitudinal force between the wheel and the ground: the adherence loss in the case of the front drive and the wheelchair rollover in the case of the rear drive. Concerning the front drive, from the vertical and moment equilibrium we obtain

$$Z_1 = \frac{a_2}{a_1 + a_2} mg - \frac{h}{a_1 + a_2} X \tag{1}$$

and, assuming incipient adherence loss, $X = fZ_1$ with f the coefficient of friction, we obtain the maximum transmittable longitudinal force for the front drive

$$X_{F,Max} = mg \frac{fa_2}{a_1 + a_2 + fh} \tag{2}$$

Concerning the rear drive, the maximum longitudinal transmittable force in the condition of incipient rollover ($Z_1 = 0$) is

$$X_{R,Max} = mg \frac{a_2}{h} \tag{3}$$

It is worth pointing out that if a hill climb is considered, the maximum slope, given in percentage, of the road that can be overcome is

$$s(\%) = 100 \frac{X}{mg} \tag{4}$$

Hence, the maximum manageable slope for front-drive is

$$s_{F,Max}(\%) = 100 \frac{fa_2}{a_1 + a_2 + fh} \tag{5}$$

and for the rear-drive is

$$s_{R,Max}(\%) = 100 \frac{a_2}{h} \tag{6}$$

TABLE 1. Reference geometry parameters of the wheelchair with the transported person.

Parameter	Value
a_1 (m)	0.8
a_2 (m)	0.2
h (m)	0.65

Considering reference geometry data of the wheelchair with the person given in Tab. 1 and the friction coefficient $f = 0.5$, we obtain $s_{F,Max} = 7.5\%$ and $s_{R,Max} = 30.8\%$. It is worth pointing out that the $s_{F,Max} < s_{R,Max}$ for any feasible value of friction coefficient f.

Hence the rear-drive configuration allows it to overcome a larger slope and will be considered for the further design of the motorized wheelchair.

B. PRELIMINARY DESIGN

Starting from the requirement related to the lack of structural modification on the wheelchair, the base idea of the project is to use external rotor motors that transmit power to the wheels of the wheelchair by friction. The equilibrium schematic of one side of the wheelchair is shown in Fig. 2, where N and T are the normal and tangential force that the motor exerts on the wheel, X and Z are the longitudinal and vertical force that the ground exerts on the wheel, and B_x and B_z are the horizontal and vertical force components at the hub of the wheel. The angular position of the motor is identified by the angle θ. Considering the system functionality, any angular position of the motor is equivalent, since the torque ($C = TR$, where R is the wheel radius) transmitted by the motor to the wheel is independent from θ. However, layout, ergonomics, and loads bearing need to be considered to choose the desired angular position of θ:

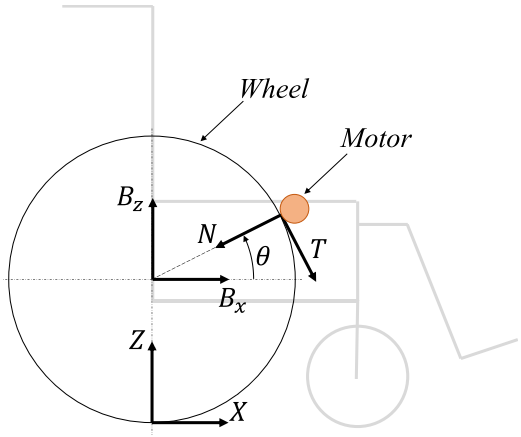

FIGURE 2. Equilibrium of a wheel of the wheelchair with motor.

1) the motor, for safety reasons, should not be placed close to the body of the person sitting on the wheelchair;
2) the motor should not interfere with the structural parts of the wheelchair;
3) the total force ($B = \sqrt{B_x^2 + B_z^2}$) acting on the wheelchair hub should be minimized, in order to reduce the load borne by the wheel axis;
4) the motor support should be connected to the wheelchair frame with easiness.

Based on these requirements, the final motor configuration was identified for $\theta = 130°$. Figure 3 shows the upper and lateral view of a reference wheelchair with the innovative plug-and-play system for electrification (shown in blue).

Each motor is pushed against the wheel by the pre-loading device, shown in Fig. 4. The pre-loading includes a glide, which can move along a rod. The motor is connected to the glide and these are pushed against the wheel of the wheelchair by a pre-load spring, which is compressed acting on a nut. The pre-loading devices, one for each wheel, are integral with an additional sub-frame, shown in Fig. 3, that can be connected to the wheelchair seat-back by means of clamps that do not require any modification of the original wheelchair. In order to allow the sub-frame to be connected to different wheelchair models, it was designed to be adjustable: indeed, the horizontal and vertical pipes of the frames are telescopic, and their length is adjustable to fit different wheelchairs.

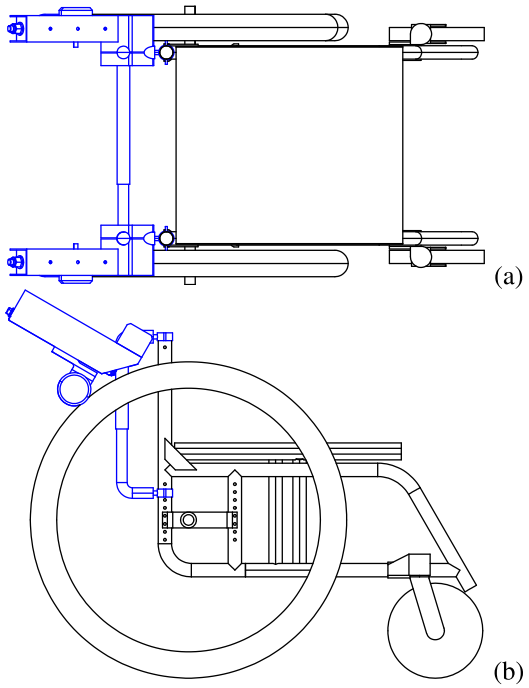

FIGURE 3. Upper (a) and lateral (b) view of the wheelchair with the innovative plug & play system for electrification (shown in blue).

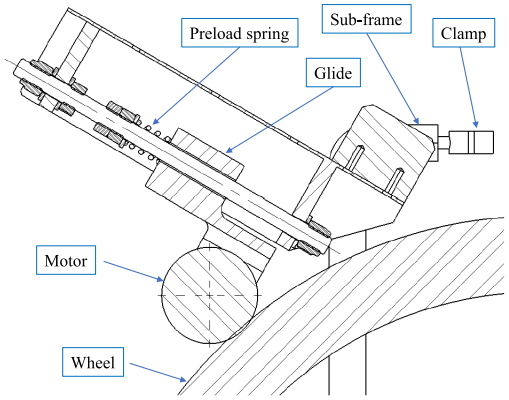

FIGURE 4. Motor to wheel pre-loading device.

Finite element simulations were performed in order to compute the stress state of the sub-frame due to the normal force and tangential force acting on the load. A trade-off between structural strength and weight was found varying the pipe thickness. Figure 6 shows the results of the equivalent von Mises stress on the final version of the sub-frame.

Finally, the wheelchair was equipped with rear safety wheels to avoid rollover.

C. TORQUE AND POWER REQUIREMENTS

In order to evaluate the torque and power requirements of the motors, two different maneuvers were considered: starting from a standstill on an uphill road to evaluate the torque and constant speed on a sloped road to evaluate the power.

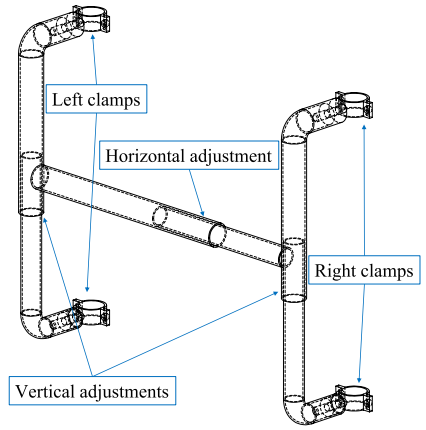

FIGURE 5. H-shaped sub-frame.

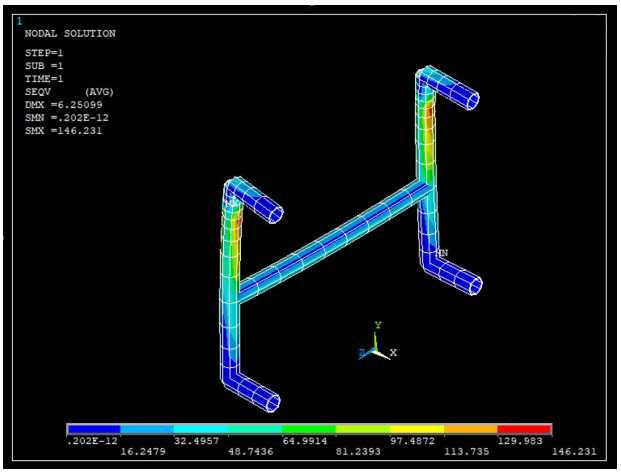

FIGURE 6. Finite element analysis of the sub-frame - Equivalent von Mises stress (MPa).

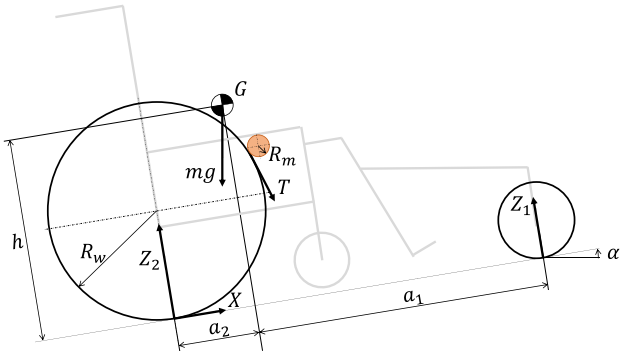

FIGURE 7. Motorized wheelchair equilibrium on a slope.

With reference to Fig. 7, in steady state condition, the magnitude of the tangential force T exerted by the motor on the wheel is equal to the traction force X, which is limited by the maximum traction force found in 3. Given the wheel radius R_w and the motor radius R_m and considering that the wheelchair is equipped with two motors, the maximum torque

required for each motor C_m^M is the following:

$$C_m^M = mg\frac{R_m a_2}{2R_w h} \tag{7}$$

To evaluate the maximum required power, we considered, in a precautionary condition, the maximum speed in correspondence with the maximum allowed road slope; its value is obtained by multiplying the maximum traction force at each wheel by the wheelchair speed, hence

$$W_m^M = mg\frac{a_2}{2h}u^M \tag{8}$$

where u^M is the maximum longitudinal speed required for the wheelchair. Considering the geometry data listed in Tab. 1, the total mass of the wheelchair (including all additional devices and transported person) $m = 150$ kg, the radius of the wheel $R_w = 0.3$ m and the radius of the motor $R_m = 0.03$ m, the maximum torque is

$$C_m^M = 22.6 \text{ Nm} \tag{9}$$

and, considering $u^M = 20$ km/h, the maximum power is

$$W_m^M = 1.3 \text{ kW} \tag{10}$$

It is worth noting that in this analysis no losses were considered, neither mechanical nor electrical. Hence, the maximum value of torque and power should be conveniently magnified in the motor choice phase.

III. PROTOTYPE PROJECT & TEST

A. SYSTEM MODELING AND PRELIMINARY SIMULATION

In the first phase of system development, the Model-Based [22], [23], [24], [25], [26] approach was used to analyze the torques required for wheelchair mobilization and validation of the Joystick mapping algorithm. In particular, a dynamic model of the wheelchair was created, and a model mapping the joystick signal to forward and spin references of the wheelchair. The primary objective is to preliminarily evaluate the choice of actuators. To do this, the model's control variables are the actuation torques at the wheels of the wheelchair. This also allows us to guide the choice of actuators by evaluating the actuation torque values required to move the wheelchair in the simulated scenarios. The construction of the dynamic model starts from the schematic representation in Fig. 8. Neglecting the effect of the motion of the pivoting front wheels, the wheelchair can in fact be thought of as a bicycle system, with the two wheels controlled. From a conceptual point of view, the fact that they are actuated on a central axis of rotation or on a parallel axis does not take away any generality, since the torques obtained are proportional to the ratio between the radius of the wheel and the radius of the motor stator. We have chosen to follow a Lagrangian approach to derive the dynamic equilibrium of the pram. In particular, we define the Lagrangian function L as the difference between the kinetic energy K and the potential

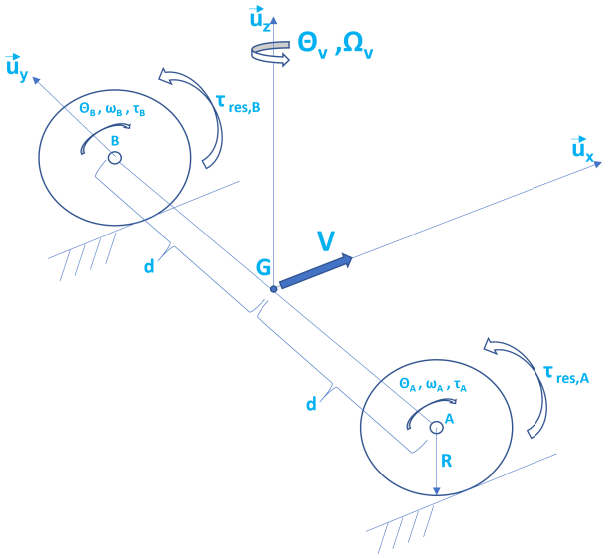

FIGURE 8. Essential representation for kinematic and dynamic modelling of wheelchair motion.

energy U of the system:

$$L \triangleq K - U \tag{11}$$

where in this case, the kinetic energy is the sum of the translation K_T and rotation K_R contributions, as follows:

$$\begin{aligned} K_T &= \frac{1}{2}m_A\left|\vec{V}_A\right|^2 + \frac{1}{2}m_B\left|\vec{V}_B\right|^2 + \frac{1}{2}M_V\left|\vec{V}_G\right|^2 \\ K_R &= \frac{1}{2}I_A\omega_A^2 + \frac{1}{2}I_B\omega_B^2 + \frac{1}{2}I_G\Omega_V^2 \end{aligned} \tag{12}$$

Note that for the mechanical system under consideration, the kinetic energy $U = U_A + U_B + U_G = (m_A + m_B + M_V)gR$ remains constant, so it can be omitted in the subsequent steps required to derive the dynamic equilibrium equations. The terms m_A, m_B and M_V and I_A, I_B, and I_G represent the masses and moments of inertia with respect to their respective axes of rotation. The expressions describing the kinematics of the bicycle are:

$$\begin{aligned} \vec{V}_A &= \vec{w}_A \wedge R\vec{u}_z = w_A R\left(\vec{u}_y \wedge \vec{u}_z\right) = w_A R\vec{u}_x \\ \vec{V}_B &= \vec{w}_B \wedge R\vec{u}_z = w_B R\left(\vec{u}_y \wedge \vec{u}_z\right) = w_B R\vec{u}_x \\ \vec{V}_G &= \vec{V}_A + \vec{\Omega}_v \wedge \overrightarrow{AG} = \vec{V}_B + \vec{\Omega}_v \wedge \overrightarrow{BG} \end{aligned} \tag{13}$$

In particular, under the assumption of rolling without creeping of both wheels, by equalising the expression of V_G starting from A and B, we derive the dependence of the wheelchair's forward speed and spin speed on the angular velocities of the wheels, as shown below.

$$w_A R - \Omega_v d = w_B R + \Omega_v d \Rightarrow \begin{cases} \Omega_v = (w_A - w_B)\frac{R}{2d} \\ V_G = (w_A + w_B)\frac{R}{2} \end{cases} \tag{14}$$

It follows that the expression of the Lagrangian function is as follows.

$$L = A\omega_A^2 + B\omega_B^2 + C\omega_A\omega_B \tag{15}$$

$$\begin{aligned} A &= \frac{m_R}{2}R^2 + \frac{M_V}{2}\frac{R^2}{4} + \frac{I_A}{2} + \frac{I_G}{2}\frac{R^2}{4d^2} \\ B &= \frac{m_R}{2}R^2 + \frac{M_V}{2}\frac{R^2}{4} + \frac{I_B}{2} + \frac{I_G}{2}\frac{R^2}{4d^2} \\ C &= M_V\frac{R^2}{4} - I_G\frac{R^2}{4d^2} \end{aligned} \tag{16}$$

Note that, with the modelling choices made, the Lagrangian function depends only on the angular velocities of the wheels, so the dynamic equations will in fact describe the dynamics of the wheels, taking into account the geometric interaction and global inertia of the vehicle.

$$\begin{aligned} \frac{d}{dt}\frac{\partial L}{\partial \dot{\omega}_A} - \frac{\partial L}{\partial \omega_A} &= Q_A^{ExT} = \tau_A - \tau_A^{\text{res}} \\ \frac{d}{dt}\frac{\partial L}{\partial \dot{\omega}_B} - \frac{\partial L}{\partial \omega_B} &= Q_B^{ExT} = \tau_B - \tau_B^{\text{res}} \end{aligned} \tag{17}$$

The terms Q_k^{ExT} are called generalised forces, which in the case of the system under consideration are given by the difference between the driving torque τ_k and the resisting torque τ_k^{res}, the expression of which is given in (18). In particular, the resistant torques are in turn the contribution of the dissipating effects of wheel-road contact friction and aerodynamic friction. In this analysis, the contribution of aerodynamic friction is ignored, given the relatively low assumed travel speed.

$$\begin{aligned} \tau_k^{\text{res}} &= \tau_{\text{friction}} + \tau_{\text{air}} \\ \tau_{\text{friction}} &= \text{sigm}\,(V_k)\,\frac{b_v}{R - b_v}\,(M_v + 2m_R)\,gR \\ &\cong \text{sign}\,(V_k)\,\frac{(M_v + 2m_R)}{20}gR \\ \tau_{\text{air}} &= \frac{1}{2}CV_G^2\,\text{sigm}\,(V_G)\,AR \cong 0 \end{aligned} \tag{18}$$

For simplicity, we considered simulations on flat sections (without tilting), so the contribution of weight force in the torques opposing the motion of the wheelchair is not considered in the equations. Combining the previous equations yields the dynamic equations describing the motion of the wheelchair with independently driven wheels. Below is the state form of the equations, which is also useful for designing a control algorithm.

$$\begin{bmatrix} \dot{\omega}_A \\ \dot{\omega}_B \end{bmatrix} = \begin{bmatrix} 2A & C \\ C & 2B \end{bmatrix}^{-1} \left(-\frac{1}{2}\begin{bmatrix} \tau_{f,A} \\ \tau_{f,B} \end{bmatrix} - \begin{bmatrix} \tau_A \\ \tau_B \end{bmatrix} \right) \tag{19}$$

Referring to the Cartesian coordinate mapping of the signal provided by the joystick, we refer to the schematic in Fig. 9. The signals coming from the joystick can be combined to generate reference signals for the control algorithm, in terms of forward and angular speed of the wheelchair, or equivalently, in reference signals for the angular speeds of the wheels being actuated. The following shows how, from Cartesian coordinates, i.e. the pair of analogue signals from the joystick (X_j, Y_j), one can switch to the equivalent representation in polar coordinates.

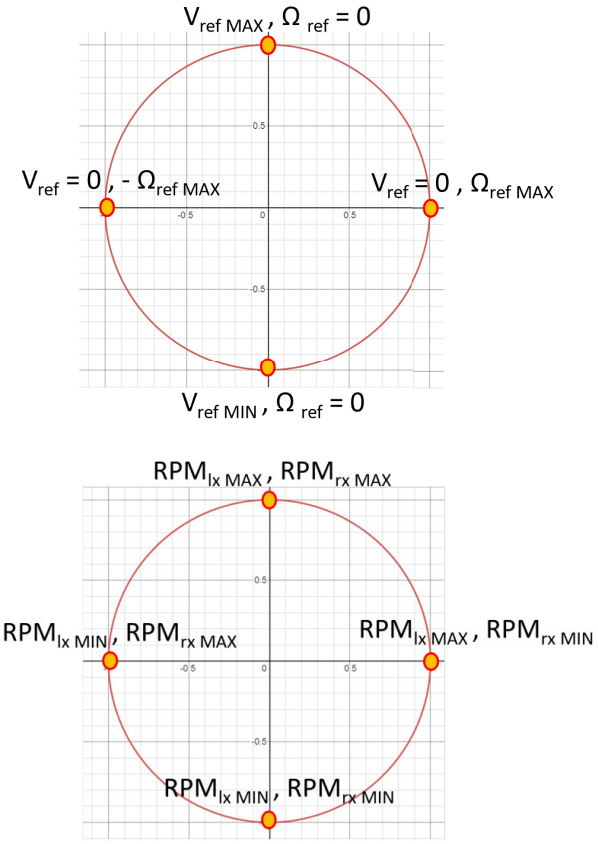

FIGURE 9. Graphical representation of joystick signal mapping in (V, Ω) (top) coordinates or, equivalently, in $(\omega_A, \omega_B) = (RPM_{lx}, RPM_{rx})$ coordinates, for convenience further converted to RPM (down).

$$\begin{pmatrix} X_j \\ Y_j \end{pmatrix} \rightarrow \begin{pmatrix} \rho = \sqrt{X_j^2 + Y_j^2} \\ \theta = \text{arctg}\left(\frac{Y_j}{X_j}\right) (\equiv k\pi) \end{pmatrix} \tag{20}$$

$$\begin{aligned} V_{\text{ref}} &= V_{\max}\sqrt{\left(\frac{X_j}{X_{\max}}\right)^2 + \left(\frac{Y_j}{Y_{\max}}\right)^2}\,\sin\left[\text{arctg}\left(\frac{Y_j}{X_j}\right)\right] \\ \Omega_{\text{ref}} &= \Omega_{\max}\sqrt{\left(\frac{X_j}{X_{\max}}\right)^2 + \left(\frac{Y_j}{Y_{\max}}\right)^2}\,\cos\left[\text{arctg}\left(\frac{Y_j}{X_j}\right)\right] \end{aligned} \tag{21}$$

Using the previous set of equations, the joystick signals were mapped into forward speed and wheelchair spin references. Then, using the previously introduced kinematic constraint equation, from the pair (V_{ref}, Ω_{ref}) it is possible to calculate references for angular velocities of the individual drive wheels, ergo references for the electric drive control that will be discussed in the following sections.

$$\begin{bmatrix} X_j \\ Y_j \end{bmatrix} \rightarrow \begin{bmatrix} V_{\text{ref}} \\ \Omega_{\text{ref}} \end{bmatrix} \rightarrow \begin{bmatrix} \omega_{A,r\ ef} \\ \omega_{B,r\ ff} \end{bmatrix} \equiv \begin{bmatrix} RPM_{lx} \\ RPM_{rx} \end{bmatrix} \tag{22}$$

To validate joystick mapping and required motors torque, we create a virtual environment in MATLAB-Simulink with

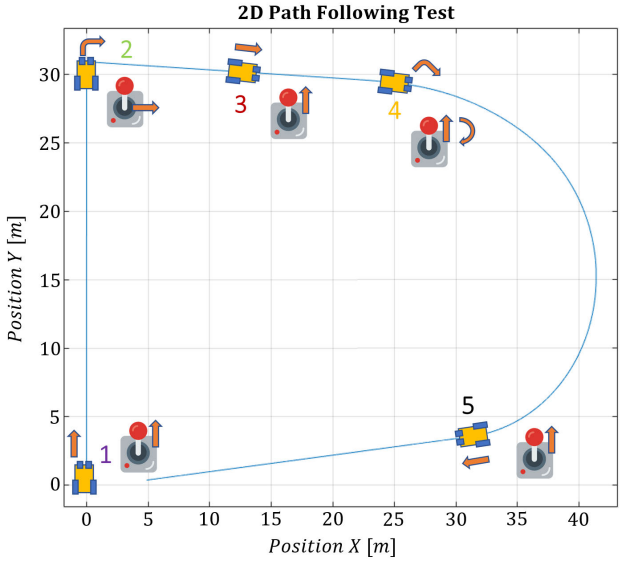

FIGURE 10. 2D trajectory and joystick reference during simulation.

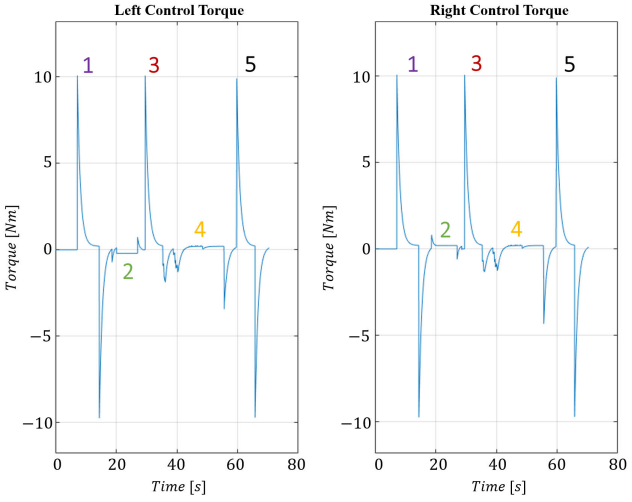

FIGURE 11. Torques applied to the left and right rear wheels during simulation.

a wheelchair model, the controller discussed above and the joystick mapping logic.

We perform the test following a reference trajectory illustrated in Figure 10 assuming flat terrain conditions. It consists mainly of five phases in which the basic movements of the joystick are tested. During the simulation, we recorded the reference and actual speed, both linear and angular - Figure 12 - set by the joystick logic to the controller, and also the torques applied to the rear wheels, presented in Figure 11. Phase 1 consists of pushing the joystick forward to its maximum extension so that the linear speed reference is set to its maximum value and the angular speed reference to zero. As a result, maximum torque is applied to both rear wheels. In phase 2, the wheelchair is stationary and is requested to rotate clockwise on the spot by pushing the joystick to the

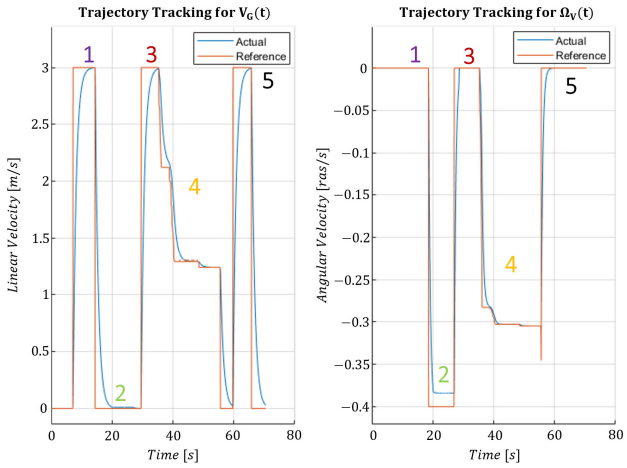

FIGURE 12. Linear and angular speed during simulation.

right. As a result, the reference linear speed is set to zero and the reference angular speed modulus to the maximum value. Since the wheelchair is asked to turn on the spot, the torques at the rear wheels must have the same modulus but opposite sign. Phase 3 consists of pushing the joystick forward again. Phase 4 consists of pushing the joystick forward and gradually rotating it approaching, without reaching, a 90° angle in a clockwise direction, maintaining maximum extension and finally returning it to its rest position. Consequently, as the joystick rotates, the linear speed reference decreases while the angular speed reference increases until the joystick returns to its resting position. Finally, phase 5 consists of pushing the joystick forward again. The results obtained prove that the joystick mapping is correct and the torque required from the motors is in line with the calculations.

B. PROTOTYPE ARCHITECTURE

The controlling logic of the automated wheelchair needs to be defined in order to map users' input to actual wheelchair movement. The second phase of prototyping aims to define a computer system architecture that will implement such logic. We start with a logical overview of the system to grasp the needed components and functionalities to move then to the slightly different physical implementation to meet usability requirements. Starting with a logical overview in Figure 13, at the core of the system we find a Micro Controller Unit (MCU). It receives information from a joystick, an Inertial Measurement Unit (IMU), an Engine Control Unit (ECU) and a touch-screen and provides commands to the ECU and telemetry information to the screen. An important role is also played by the ECU, which manages engine rotation. Specifically, the ECU receives target speed reference commands from the MCU and manages the process of reaching these target speeds.

As concerning the MCU, an esp32-wroom-32d [27] is selected. It is a low-cost MCU that integrates a Bluetooth Low Energy (BLE) module for wireless communication and

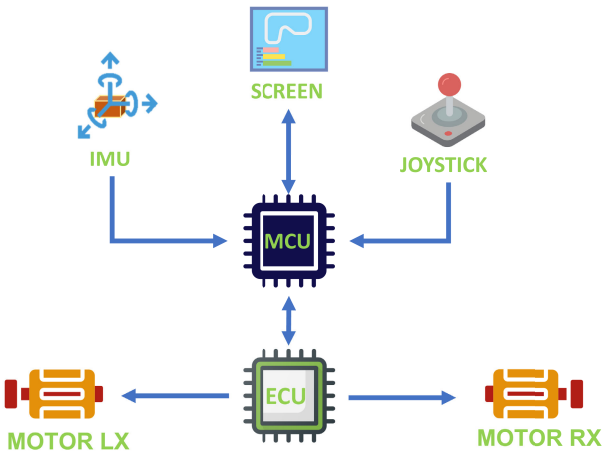

FIGURE 13. Logical view of the system. Image: flaticon.com.

provides a port of FreeRTOS [28] into its official ESP-IDF [29] development framework. Available peripheral interfaces include I2C [30], UART [31], SPI [31]. In addition, it incorporates cryptographic hardware acceleration which allows secure communications to still be efficient. It embeds also two low-power Xtensa® 32-bit LX6 microprocessors which can run independent threads at the same time.

Regarding the ECU, a Vedder ESC 100A is selected. It is an open-source electronic speed controller [32] used in electric skateboards, electric bikes, and other electric vehicles. The VESC system was developed by Benjamin Vedder, and it is based on the STM32 microcontroller platform. The VESC allows for precise control of the motor's speed and torque, and it includes a variety of features such as regenerative braking and motor temperature monitoring. The VESC system is highly customizable and programmable, making it popular among DIY enthusiasts and manufacturers of electric vehicles. The VESC uses a technique called Field Oriented Control (FOC) [33], [34], [35], [36] to control the speed and torque of the motor. FOC is a control strategy that separates the stator current of the motor into two components: one component that generates the magnetic field and another component that generates the torque. This separation allows the VESC to control the motor's speed and torque independently. The VESC uses a PI (proportional-integral) control algorithm to regulate the motor's speed and torque. The PI controller continuously compares the desired motor speed/torque to the actual motor speed/torque and adjusts the motor's current accordingly. The proportional term of the PI controller responds to the current error (the difference between the desired and actual current) by applying a current proportional to the error. The integral term responds to the accumulated error over time and helps to eliminate any steady-state error. In addition to the PI controller, the VESC uses several other techniques to improve motor control, such as: (i) Sensorless Control: The VESC can operate the motor without using traditional Hall sensors, which simplifies the design and reduces costs. (ii) FOC Field Weakening: As the motor's speed increases, the maximum torque the motor can produce decreases. The VESC uses a technique called FOC field weakening to maintain the maximum torque output of the motor as the speed increases. (iii) Dynamic Braking: The VESC can use the motor to slow down the vehicle by regenerating energy back into the battery, which reduces wear on the brakes and increases the vehicle's range. Overall, the VESC's control algorithm is designed to provide precise and efficient control of the motor's speed and torque, while also maximizing the vehicle's performance and energy efficiency. Thanks also to its wide input voltage range and remarkable continuous output working current specified in Table 2, it represents a suitable option for small-medium power motor-propelled prototypes.

TABLE 2. VESC 100A specification.

Characteristic	Value
Input voltage	14-84V (4-20S)
Continuous Current	100A
Max Current	120A
Control Interface Ports	USB, CAN, UART
BEC	5V@1A
Modes	DC, BLDC, FOC (sinusoidal)
Input Set Support	PPM, ADC, NRF, UART

Concerning the screen, a Nextion nx4827t043 [37] is selected. This is a touch-screen so there is a possibility to provide virtual and adjustable buttons for better accessibility.

For the joystick, a DM11L0A1F [38] is selected and depicted in Figure 14. This is a 2-axis resistor joystick that exploits two potentiometers to represent the stick position.

FIGURE 14. DM11L0A1F 2-axes resistor joystick. Terminals VDD, GND and OUT are visible on two edges of the joystick.

For the IMU, an ICM-20948 [39] is selected because of its low cost and its Digital Motion Processor that takes care of the calibration of embedded sensors. Thanks to its 3-axis gyroscope, 3-axis accelerometer, and 3-axis magnetometer, it is able to provide accurate pitch, roll and yaw of the vehicle. Its usage is discussed later.

For motors, two MBoards 6374 180KV [40] are chosen and depicted in Figure 15. Their specifications in Table 3 fulfil the requirements of dimension and power needed by mechanical requirements. They can also be controlled by the selected ECU so that they represent a perfect candidate for the application.

To power the system, a battery must be chosen. Since it will be connected to a VESC, it must match its permitted input

FIGURE 15. Mboards motor 180kv.

TABLE 3. Motor specification.

Characteristic	Value
Motor KV	180kv
Motor type	outrunner
Motor Wind	13
Idle current	1.7A
Motor Resistance	0.053Ohm
Max. Power	3250W
ESC	80-100A
Pole Pairs	7
Dimension (L*W)	(63*74)mm

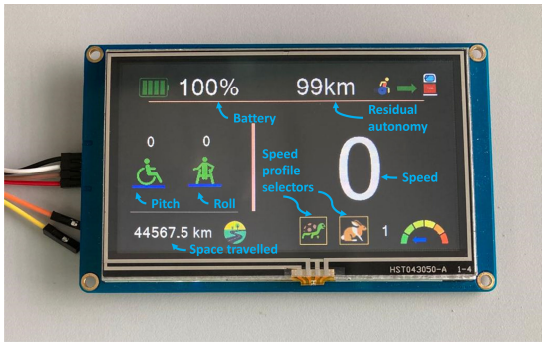

FIGURE 16. Example of possible GUI.

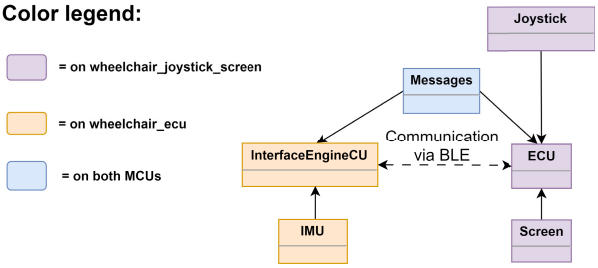

FIGURE 17. Overview of classes distributed among the two microcontrollers. Arrows pointing towards one class mean that the pointed class is using the other class.

characteristics. For this reason, a 10s3p P42A battery [41] is chosen. This is a 10s3p lithium-ion battery with a nominal voltage of 36V. Considering the selected motors and VESC characteristics, two independent batteries are mounted which are able to exploit all motors' power being able to sustain the maximum allowed current.

In our application, we want to exploit an IMU to obtain so-called attitude and heading reference systems (AHSR), i.e. pitch, roll, and yaw of the vehicle, so that safety policies can be implemented based on the stability of the wheelchair. By integrating the IMU with the wheelchair, it becomes feasible to identify instances of tipping and establish appropriate measures to address such occurrences. Various options can be considered, such as integrating a GPS module to provide location information or emitting audible signals to alert individuals in proximity. Additionally, there is the possibility of automatically deactivating the wheelchair's engines.

The screen is part of the Human-Computer Interface (HMI) and it is used to visualize important information the user needs to monitor such as current speed, remaining percentage of battery, pitch and roll of the wheelchair, and current selected speed profile. If empowered by touchscreen capability, the screen can be used not only as an output device but also as an input one. Therefore, we could avoid physical buttons or at least they may coexist. An example of Graphical User Interface (GUI) [42] can be observed in Figure 16.

The system we are dealing with is a real-time system because the correctness of the result depends not only on the correctness of the calculation but also on temporal correctness. Just as an example, the command to brake the wheelchair will not be considered as correct if it will eventually be processed after a collision. To grant the satisfaction of each deadline, we make use of a Real-Time Operating System. Among the RTOS available implementations, freeRTOS [43] is chosen.

While there are alternative options available, the decision was made to utilize the freeRTOS operating system on the esp32 microcontroller due to the existence of an official port. To schedule application-defined tasks, an RTOS uses a scheduling algorithm to decide which tasks should be executed in a specific time interval. Among the scheduling algorithms available for freeRTOS, it is selected Prioritized Preemptive Scheduling with Time Slicing whose configuration is reported in Table 4.

TABLE 4. Configuration parameters for Prioritized Preemptive Scheduling with Time Slicing in freeRTOS.

Constant	Value
configUSE_PREEMPTION	1
configUSE_TIME_SLICING	1

The idea is that in the event that a task with a higher priority is ready to be executed, it will use the pre-emption mechanism to enter into operation. Configuring the kernel to utilise time slicing allows round-robin scheduling to be implemented, since at each time unit, the scheduling algorithm will select a new task to enter the execution state if there are other tasks ready with the same priority as the executing task.

Considering usability as an important metric of our system, we decided to develop a wireless controller. For this reason, the physical view of the system in Figure 18 is different from

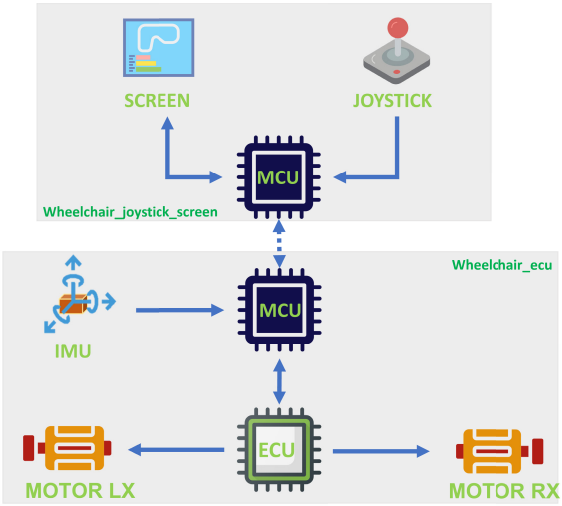

FIGURE 18. Physical view of the system. Image: flaticon.com.

the logical one in Figure 13. In this configuration, an MCU is in charge of handling input from joystick and screen and displaying telemetry information to the screen whereas another one is handling the ECU and IMU. Both MCUs communicate using a custom BLE protocol appropriately designed for this application. A detailed discussion is carried out in the software architecture chapter.

C. SOFTWARE ARCHITECTURE

The third phase of our prototyping aims to define the architecture of the software which will run on MCUs. The application of the encapsulation concept, derived from object-oriented programming style [44], led us to design several classes as represented in Figure 17.

From a high-level perspective, each physical component has a related class that hides its complexity. In this way, there is no binding on the use of a particular brand: as long as there is an implementation of the declared interface, every physical component is fine. This approach is also useful for decoupling software to improve debugging and testing. Given a component to be tested, since there is no code directly relating to other components, but only a reference to their classes, it is easier to mock any reference to external components. In this way, only the logic of the component under test is tested. Furthermore, in case of a software module has a bug within it or needs an update of its logic, this can be done without the need to update the other components as well, as long as its interface remains the same.

Based on the physical view in Figure 18, we find a similar organisation in the code. According to the physical view, there are two microcontrollers running two independent instances of the freeRTOS firmware. There are object classes, distributed on only one of the two microcontrollers and some distributed on both. By looking at the legend in Figure 17, we can see which object classes are distributed on which microcontroller.

The IMU class offers methods to retrieve AHSR references or individual values, depending on the need. In addition, methods to configure sensors via a constructor and a way to update the values returned by each embedded sensor.

The InterfaceEngineCU is the class in charge of communicating directly with the ECU. Since communication is via a UART communication, it provides a method for configuring all related parameters such as baud rate, parity check, communication pins, etc. To control the motors, it offers methods to set the RPM and a method for obtaining information from the engines themselves via a protocol defined by the ECU manufacturer. The motor's rotation references come from the previously discussed mapping that takes as input the values indicated by the joystick, which is controlled by the other microcontroller. As already mentioned, communication takes place via BLE and therefore the class offers a method to set up communication.

The ECU class is a mirror of InterfaceEngineCU distributed on the microcontroller in charge of managing the joystick. It offers a method of communication via BLE to set the RPM references of the motors, calculated from the joystick mapping. It also offers a method for setting the speed level to customise different driving styles.

The Joystick class offers methods to manage a 2-axis resistive joystick. It provides access to both low-level information from the potentiometers connected to the joystick, as well as high-level information such as Cartesian coordinates and polar coordinates of the stick position in a 2-D Cartesian plane. Therefore, internally the class object must define a strategy to handle noisy values, such as those coming from the esp32's ADC. Our strategy consists of applying a median filter to smooth out the scattered values returned by the ADC, trying to preserve their trend as much as possible. The particular values of the median filter were found using a fine-tuning approach. Moreover, in order to reduce the sensitivity of the joystick to produce an RPM reference different from zero only when a clear intention of movement is detected, a circular dead zone around the centre of the cartesian plane has been applied. Only when the position of the joystick stick exceeds this dead zone is its position considered different from the origin.

The Screen class hides the details of physical communication with the screen and offers methods for setting telemetry information to be displayed, such as remaining battery level, stability information, etc. It also allows listening to events, such as touches on virtual buttons.

The Messages class hides all the details of how messages are exchanged and provides methods for defining callbacks. These callbacks enable the processing of received messages and the delivery of the contained information without requiring direct manipulation of the message handling mechanisms. The format of the messages that the two microcontrollers exchange is illustrated in Figure 19.

Each message is characterised by an opcode and a payload. Depending on the opcode, the payload can change in the number of fields and the types of data contained.

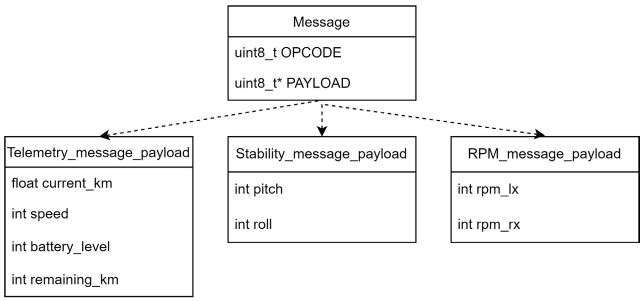

FIGURE 19. Message format exchanged via BLE with some examples of payloads related to the application logic.

Obviously, each microcontroller must know the list of all possible message opcodes and the corresponding structure of the contained payload.

The programming language used to implement the software is C++, although Micropython is an alternative for ESP32 boards.

C++ code for both MCUs and complete UML class diagrams are made available on GitHub at sources [45], [46].

D. PROTOTYPE IMPLEMENTATION

To test the system, a rapid implementation has been carried out. As discussed so far, the system consists of two subsystems. The joystick-screen-MCU subsystem communicates wirelessly with the other subsystem and is powered by a power bank. For the greatest possible flexibility, it can be used attached to the armrest of the wheelchair or not. The subsystem is therefore enclosed in a plastic box printed with a 3D printer, which can be seen in Figure 20.

FIGURE 20. Subsystem joystick-screen-MCU with USB cable for power supply.

The other subsystem, consisting of MCU-IMU-ECU, is attached to the wheelchair. Specifically, using a breadboard, the MCU, the IMU, and the connectors were soldered in order to connect the MCU and the ECU, visible in Figure 21. For safety reasons, this subsystem is hidden inside a plastic box where there is also the battery.

The final system, shown in Figure 22, was tested in a real-world scenario for a total of 20 hours on uneven terrain with a maximum slope of 10%. For simplicity, we report two representative experiments. The test conditions were

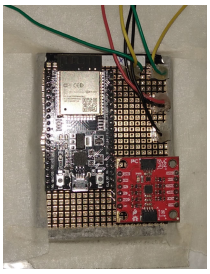

FIGURE 21. Implementation of IMU-ESP32 system.

FIGURE 22. Wheelchair with plug-and-play kit.

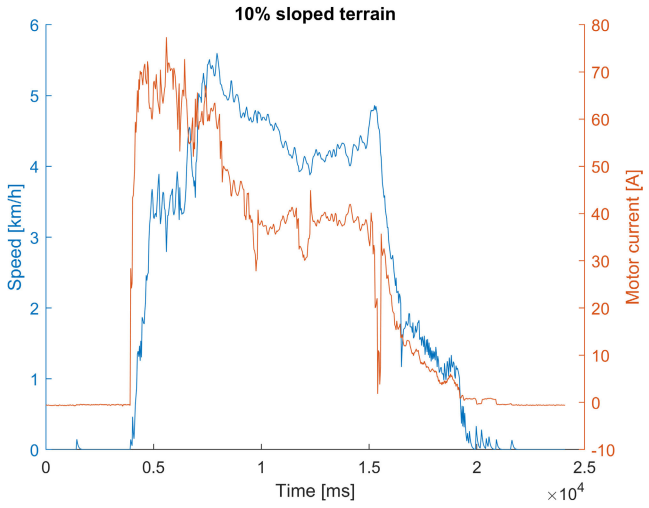

FIGURE 23. Profile in time of left motor current and wheelchair speed during a test on a 10% sloped terrain.

as follows: driver's weight of 70 kg, fully charged battery, straight trajectory, zero initial speed.

Considering an experiment on a 10% sloped terrain - Figure 23 - the system was driven a total of 19 metres. When the user pushes the joystick forward, the system regulates the current of the motors to reach the desired speed. Since the trajectory is following a straight line, the graph

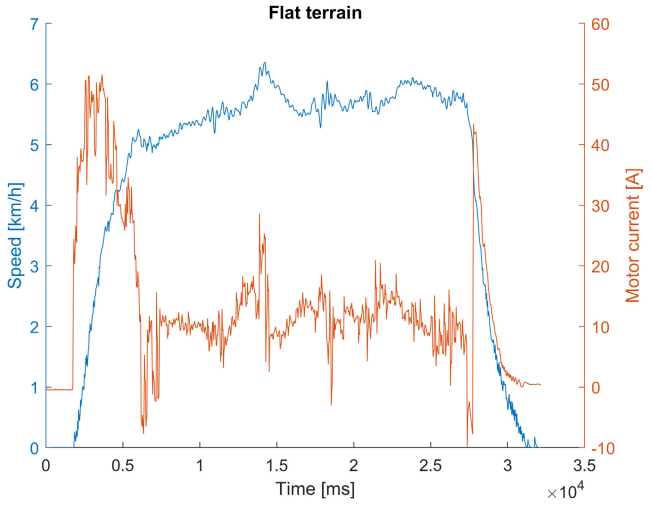

FIGURE 24. Profile in time of left motor current and wheelchair speed during a test on flat terrain.

of only one motor was shown because the two profiles are identical. The initial behaviour shows a current peak to overcome the inertia of the system. The maximum peak is approximately 77A. Assuming a fully charged battery, i.e. with a voltage of 41V, the system requires a peak of about 3150W. To maintain an average speed of 4.5 km/h, the system requires 1700W per motor. Considering another experiment on flat terrain - Figure 24 - the system was driven a total of 41m. Looking at the figure, in the same way as observed in the previous experiment, a prominent peak can be observed, indicating the initial movement. However, on average, the required current is lower, as there is no contribution from the slope. The maximum peak current is about 50A. Assuming a fully charged battery, the system requires a peak of about 2050W per motor. To maintain an average speed of 5.6 km/h, the system requires approximately 465 W per motor.

IV. CONCLUSION

Self-propelled wheelchairs are difficult to drive on off-road routes or require enormous physical effort in situations where the gradient exceeds 8%. For most people, these situations are too strenuous and therefore impractical. This paper presented an innovative plug-and-play system to electrify a manual wheelchair. We discussed the mechanical design, with the prerequisite of making no changes to the original wheelchair, to allow the wheelchair to be propelled by friction by two motors in contact with the rear wheels. For validation, a model has been developed and checked through simulation. We discussed a prototype architecture for the control system and its software architecture. Finally, we presented a prototype implementation tested for a total of 20 hours in a real scenario over uneven terrain with a maximum peak gradient of 10%. The driving experience was comfortable and the system followed smoothly the joystick input.

The use case behind the development of this project was to enable people with wheelchairs to visit places of interest with off-road routes and/or distances not suitable for manual wheelchairs. With this work, the foundations were laid for a wheelchair-adaptable support that, with reversible bindings, allows people to present themselves at the place of interest with their wheelchair and have the kit assembled on site. Thanks to the simple design, assembly can also be carried out by inexperienced users. Currently, to the best of our knowledge, there is no kit that can fulfil this need.

As future work, tests will be carried out with disabled people with different kinds of functioning [47]. The HMI can be easily adapted accordingly. In addition, if this kit were adopted by tourist attractions that fall under the above-mentioned conditions, it would offer people with manual wheelchairs the opportunity to visit independently without the need to present themselves with an electric wheelchair or an electrification kit, provided they have one available, thus reducing the problems associated with travelling.

REFERENCES

[1] J. Beard, S. Biggs, D. E. Bloom, L. P. Fried, P. R. Hogan, A. Kalache, and S. J. Olshansky. (Jan. 2012). *Global Population Ageing: Peril or Promise?* Program Global Demography Aging, PGDA Work. [Online]. Available: https://ideas.repec.org/p/gdm/wpaper/8912.html

[2] C. L. Flemmer and R. C. Flemmer, "A review of manual wheelchairs," *Disab. Rehabil., Assistive Technol.*, vol. 11, no. 3, pp. 177–187, Apr. 2016, doi: 10.3109/17483107.2015.1099747.

[3] B. Pierret, K. Desbrosses, J. Paysant, and J.-P. Meyer, "Cardio-respiratory and subjective strains sustained by paraplegic subjects, when travelling on a cross slope in a manual wheelchair (MWC)," *Appl. Ergonom.*, vol. 45, no. 4, pp. 1056–1062, Jul. 2014.

[4] E. G. Collins, D. Gater, J. Kiratli, J. Butler, K. Hanson, and W. E. Langbein, "Energy cost of physical activities in persons with spinal cord injury," *Med. Sci. Sports Exercise*, vol. 42, no. 4, pp. 691–700, 2010.

[5] A. R. Meyers, J. J. Anderson, D. R. Miller, K. Shipp, and H. Hoenig, "Barriers, facilitators, and access for wheelchair users: Sbstantive and methodologic lessons from a pilot study of environmental effects," *Social Sci. Med.*, vol. 55, no. 8, pp. 1435–1446, Oct. 2002.

[6] D. Reid, D. Laliberte-Rudman, and D. Hebert, "Impact of wheeled seated mobility devices on adult users' and their caregivers' occupational performance: A critical literature review," *Can. J. Occupational Therapy*, vol. 69, no. 5, pp. 261–280, Dec. 2002.

[7] I. Domingues, J. Pinheiro, J. Silveira, P. Francisco, J. Jutai, and A. C. Martins, "Psychosocial impact of powered wheelchair, users' satisfaction and their relation to social participation," *Technologies*, vol. 7, no. 4, p. 73, Oct. 2019. [Online]. Available: https://www.mdpi.com/2227-7080/7/4/73

[8] C. Torkia, D. Reid, N. Korner-Bitensky, D. Kairy, P. W. Rushton, L. Demers, and P. S. Archambault, "Power wheelchair driving challenges in the community: A users' perspective," *Disab. Rehabil., Assistive Technol.*, vol. 10, no. 3, pp. 211–215, May 2015, doi: 10.3109/17483107.2014.898159.

[9] Triride. *MTW Trekking Power*. Accessed: Nov. 4, 2023. [Online]. Available: https://www.trirideitalia.com/mtw-multi-traction-wheelchair/mtw-trekking-power/

[10] Empulse. *F55 With 14" Rear Wheel*. Accessed: Apr. 11, 2023. [Online]. Available: https://www.sunrisemedical.de/elektromobilitaet/empulse/rollstuhl-zuggeraete/f55-14-version

[11] Alber. *E-Motion*. Accessed: Apr. 11, 2023. [Online]. Available: https://www.alber.de/en/products/active-drives/e-motion/#produktaufbau-lieferumfang

[12] AAT. *MAX-E*. Accessed: Apr. 11, 2023. [Online]. Available: https://www.aat-online.de/gb/rehabilitation-gb/drive-gb/max-e-start-gb.html
[13] Benoit System. *Light Drive*. Accessed: Apr. 11, 2023. [Online]. Available: https://benoitsystemes.com/en/minotor2.php
[14] Max Mobility. *Smart Drive MX2*. Accessed: Apr. 11, 2023. [Online]. Available: https://progettiamoautonomia.it/prodotto/smart-drive/
[15] R. Mejía-Gutierréz and D. Zuluaga-Holguín, "Design of an electrical power assist kit for manual wheelchair under the conditions of developing countries," in *Proc. Int. Conf. Eng., Technol. Innov. (ICE) IEEE Int. Technol. Manag. Conf.*, Jun. 2013, pp. 1–11.
[16] N. N. Kumar, S. Patil, Prabhudeva, S. Nair, and K. T. Prajwal, "Design and development of smart portable gadget for mobility," in *Proc. 6th Int. Conf. Trends Electron. Informat. (ICOEI)*, Apr. 2022, pp. 01–06.
[17] X. Jin, J. Wang, X. He, Z. Yan, L. Xu, C. Wei, and G. Yin, "Improving vibration performance of electric vehicles based on in-wheel motor-active suspension system via robust finite frequency control," *IEEE Trans. Intell. Transp. Syst.*, vol. 24, no. 2, pp. 1631–1643, Feb. 2023.
[18] X. Jin, J. Wang, Z. Yan, Z. Li, and Z. Wang, "Development of robust constrained control strategy for active suspension system of electric vehicle with in-wheel-motor," in *Proc. 40th Chin. Control Conf. (CCC)*, Jul. 2021, pp. 6172–6177.
[19] X. Jin and Q. Wang, "Nonlinear robust control of trajectory-following for autonomous ground electric vehicles," in *Electric Vehicles—Design, Modelling and Simulation*, D. N. Tudoroiu, Ed. Rijeka, Croatia: IntechOpen, 2023, ch. 3, doi: 10.5772/intechopen.112049.
[20] X. Jin, Z. Yan, G. Yin, S. Li, and C. Wei, "An adaptive motion planning technique for on-road autonomous driving," *IEEE Access*, vol. 9, pp. 2655–2664, 2021.
[21] B. D. Matteo, D. Fanucci, F. Mondini, and N. Pacini, "Dispositivo di motorizzazione per sedia a rotelle," Italy Patent Application for Utility model 16 515 979, Jun. 7, 2022.
[22] P. Dini and S. Saponara, "Model-based design of an improved electric drive controller for high-precision applications based on feedback linearization technique," *Electronics*, vol. 10, no. 23, p. 2954, Nov. 2021.
[23] C. Bernardeschi, P. Dini, A. Domenici, and S. Saponara, "Co-simulation and verification of a non-linear control system for cogging torque reduction in brushless motors," in *Software Engineering and Formal Methods*. Oslo, Norway: Springer, 2020, pp. 3–19.
[24] F. Cosimi, P. Dini, S. Giannetti, M. Petrelli, and S. Saponara, "Analysis and design of a non-linear MPC algorithm for vehicle trajectory tracking and obstacle avoidance," in *Applications in Electronics Pervading Industry, Environment and Society*. Berlin, Germany: Springer, 2021, pp. 229–234.
[25] C. Bernardeschi, P. Dini, A. Domenici, A. Mouhagir, M. Palmieri, S. Saponara, T. Sassolas, and L. Zaourar, "Co-simulation of a model predictive control system for automotive applications," in *Software Engineering and Formal Methods, SEFM 2021 Collocated Workshops*. Berlin, Germany: Springer, 2022, pp. 204–220.
[26] P. Dini and S. Saponara, "Processor-in-the-loop validation of a gradient descent-based model predictive control for assisted driving and obstacles avoidance applications," *IEEE Access*, vol. 10, pp. 67958–67975, 2022.
[27] (2023). *ESP32-WROOM-32D& ESP32-WROOM-32U Datasheet*. Espressif Systems. [Online]. Available: https://www.espressif.com/sites/default/files/documentation/esp32-wroom-32d_esp32-wroom-32u_datasheet_en.pdf
[28] *RTE*. Accessed: Apr. 11, 2023. [Online]. Available: https://www.freertos.org/
[29] Espressif. *ESP-IDF Programming Guide*. Accessed: Apr. 11, 2023. [Online]. Available: https://docs.espressif.com/projects/esp-idf/en/latest/esp32/
[30] Philips Semiconductors. *I2C Specification*. Accessed: Apr. 11, 2023. [Online]. Available: https://www.i2c-bus.org/specification/
[31] D. S. Dawoud and P. Dawoud, *Serial Communication Protocols and Standards*. Gistrup, Denmark: River, 2020.
[32] B. Vedder. *VESC-Project*. Accessed: Apr. 11, 2023. [Online]. Available: https://vesc-project.com/
[33] P. Dini and S. Saponara, "Cogging torque reduction in brushless motors by a nonlinear control technique," *Energies*, vol. 12, no. 11, p. 2224, Jun. 2019.
[34] P. Dini and S. Saponara, "Design of adaptive controller exploiting learning concepts applied to a BLDC-based drive system," *Energies*, vol. 13, no. 10, p. 2512, May 2020.
[35] P. Dini and S. Saponara, "Design of an observer-based architecture and non-linear control algorithm for cogging torque reduction in synchronous motors," *Energies*, vol. 13, no. 8, p. 2077, Apr. 2020.
[36] C. Bernardeschi, P. Dini, A. Domenici, M. Palmieri, and S. Saponara, "Formal verification and co-simulation in the design of a synchronous motor control algorithm," *Energies*, vol. 13, no. 16, p. 4057, Aug. 2020.
[37] *NX4827T043 Datasheet*. Nextion. Accessed: Apr. 11, 2023. [Online]. Available: https://www.analog.com/media/en/technical-documentation/data-sheets/3600fd.pd
[38] *Miniature Resistive Joysticks Datasheet*. APEM. Accessed: Apr. 11, 2023. [Online]. Available: https://docs.rs-online.com/b890/0900766b81297a18.pdf
[39] (2017). *ICM-20948 Datasheet*. TDK InveSense. [Online]. Available: https://invensense.tdk.com/wp-content/uploads/2016/06/DS-000189-ICM-20948-v1.3.pdf
[40] MBoards. *Motors 6374 Specifications*. Accessed: Apr. 11, 2023. [Online]. Available: https://www.mboards.co/products/mboards-6374-180kv-motor
[41] MBoards. *Motors 10S3P P42A Battery Pack*. Accessed: Apr. 11, 2023. [Online]. Available: https://www.mboards.co/collections/batteries/products/10s3p-p42a-battery-pack-transparent-series
[42] D. Benedetti, J. Agnelli, A. Gagliardi, P. Dini, and S. Saponara, "Design of a digital dashboard on low-cost embedded platform in a fully electric vehicle," in *Proc. IEEE Int. Conf. Environ. Electr. Eng. IEEE Ind. Commercial Power Syst. Eur.*, Jun. 2020, pp. 1–5.
[43] RTE. *The Freertos Reference Manual: API Functions and Configuration Options*. Accessed: Apr. 11, 2023. [Online]. Available: https://www.freertos.org/Documentation/RTOS_book.html
[44] Cppreference.com. *Encapsulation*. Accessed: Apr. 11, 2023. [Online]. Available: https://en.cppreference.com/book/intro/encapsulation
[45] F. Pacini. (Jan. 2023). *Wheelchair ECU*. [Online]. Available: https://github.com/FedePacio97/wheelchair_ecu
[46] F. Pacini. (Jan. 2023). *Wheelchair Joystick Screen*. [Online]. Available: https://github.com/FedePacio97/wheelchair_joystick_screen
[47] *International Classification of Functioning, Disability and Health: ICF: Short Version*, World Health Organization, Geneva, Switzerland, 2001.

FEDERICO PACINI received the B.S. and M.S. degrees in computer engineering from the University of Pisa (UNIPI), in 2019 and 2021, respectively, where he is currently pursuing the Ph.D. degree in information engineering, under the supervision of Prof. Luca Fanucci. His current research interest includes advanced assistive technologies integrating artificial intelligence algorithms for cooperative driving systems.

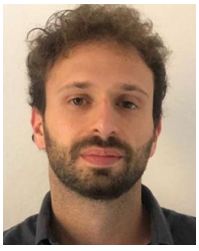

STEFANO DI MATTEO received the Ph.D. degree (cum laude) in information engineering from the University of Pisa, in 2023. He is currently a Postdoctoral Researcher with the University of Pisa. His current research interests include digital and VLSI designs and embedded systems for cybersecurity and cryptography in different application fields (automotive, HPC, and the IoT).

PIERPAOLO DINI received the master's degree in automation engineering and the Smart Industry Ph.D. degree (Hons.) from the University of Pisa (UNIPI). He is currently a Postdoctoral Researcher with the Department of Information Engineering, UNIPI. He collaborates in multiple European research projects focused on the development of advanced control and monitoring algorithms for mechatronic systems in industrial applications. His current research interests include control systems technology, advanced control theory, and innovative model-based design paradigms with applications in power electronics and electric drives.

LUCA FANUCCI (Fellow, IEEE) received the Laurea and Ph.D. degrees in electronic engineering from the University of Pisa, in 1992 and 1996, respectively. From 1992 to 1996, he was with the European Space Agency, ESTEC, Noordwijk, The Netherlands, as a Research Fellow. From 1996 to 2004, he was a Senior Researcher with the Italian National Research Council, Pisa. He is currently a Full Professor of microelectronics with the University of Pisa. He is the coauthor of more than 500 journal articles and conference papers and a co-inventor of more than 40 patents. His current research interests include several aspects of design technologies for integrated circuits and electronic systems, with an emphasis on system-level design, hardware/software co-design, and sensor conditioning and data fusion. His main application areas are in the field of wireless communications, low-power multimedia, automotive, healthcare, ambient assisted living, and technical aids for independent living. He is a member of the editorial board of *Technology and Disability* (IOS Press). He is a fellow of DATE. He served on several technical program committees for international conferences. He was the Program Chair of the 2008 DSD and the 2014 DATE and the General Chair of the 2016 DATE and the 2020 HIPEAC.

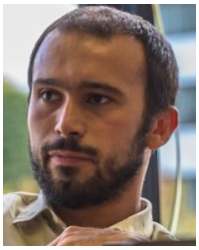

FRANCESCO BUCCHI received the M.Sc. degree in vehicle engineering and the Ph.D. degree in mechanical engineering from the University of Pisa, in 2014. He has been an Associate Professor of machine design with the University of Pisa, since 2021, where he is currently a Teacher of the course automotive design. The Ph.D. thesis deals with smart materials for automotive applications. His current research interests include the mechanics of materials and the design and simulation of vehicles, vehicle components, and transported goods.

Open Access funding provided by 'Università di Pisa' within the CRUI CARE Agreement